

Development of Polar BODIPY-Tetrazines for Rapid Pretargeted Fluorescence Imaging

Markus Staudt, Lars Hvass, Marius Müller, Rocío García-Vázquez, Jesper Tranekjær Jørgensen, Vladimir Shalgunov, Umberto Maria Battisti, Andreas Kjær,* and Matthias M. Herth*



Cite This: *ACS Omega* 2024, 9, 42498–42505



Read Online

ACCESS |



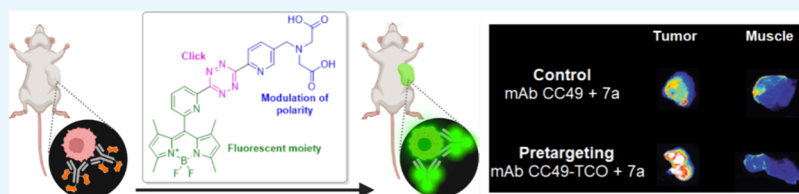
Metrics & More



Article Recommendations



Supporting Information



ABSTRACT: Polar BODIPY-tetrazine dyes were developed and clicked in vivo to a preaccumulated *trans*-cyclooctene-modified anti-TAG72 monoclonal antibody CC49 (CC49-TCO). The in vivo click performance was evaluated using an in-house developed ex vivo blocking assay. All tested polar BODIPY structures exhibited excellent in vivo binding, confirming that the turn-on tetrazine dyes successfully clicked in vivo to pretargeted CC49-TCO. Fluorescence imaging showed high tumor-to-muscle ratios of 4:1. This proof-of-concept study indicates that the pretargeting concept based on turn-on probes could be used for cancer treatments, such as photodynamic or -thermal therapy.

INTRODUCTION

Fluorescence intraoperative guided surgery (FIGS) and photodynamic and -thermal therapies are gaining increasing attention within academic and clinical settings.^{1–5} Due to their nonspecific biodistribution, these fluorophores are often covalently linked to well-established receptor-targeting vectors to reach the desired target sites. Promising clinical results could be achieved with monoclonal antibodies conjugated to fluorescent dyes.^{6,7}

However, the slow clearance of large antibodies leads to considerable and unavoidable background signal. In the case of photodynamic and -thermal therapies, this can lead to side effects, such as sensitivity of skin and eyes to bright lights and sunlight.^{8,9} Furthermore, the often charged fluorophores conjugated to the established antibodies lead to large changes in their pharmacokinetics.¹⁰ While higher dye loads lead to increased fluorescence, the pharmacokinetic changes become even more profound.^{11,12} Clinical translation is therefore often hampered by insufficient biodistribution data. Proper target accumulation and treatment success cannot be assessed before initiating the therapy.¹³ Recently, it has been shown that pretargeting strategies can be used to track the biodistribution of mAbs for therapeutic and diagnostic reasons.^{14,15} Pretargeting is based on a two-step approach where, first, a tagged mAbs, usually using *trans*-cyclooctene (TCO), is allowed to accumulate at its target and excrete from the rest of the body; in the second step, a tetrazine (Tz)-based imaging agent is administered, which bioorthogonally reacts with the tag of the mAbs (Figure 1B).¹⁶ Due to the rapid click reaction between

the Tz and TCO (typical rate constants of $>50,000 \text{ M}^{-1} \text{ s}^{-1}$) and the fast excretion of unreacted Tzs, good target-to-background ratios (TBRs) have been achieved that are up to 10-fold higher compared to those of conventionally directly labeled mAb approaches.¹⁴ The use of clearing or masking agents can increase this contrast even further up to 150-fold.¹⁷ Interestingly, Tzs also find applications in fluorescence imaging. Turn-on fluorophore Tzs activate fluorescence after the reaction with TCOs, resulting in strong signal amplification of up to 10^3 -fold.^{18,19} The resulting low background signal leads to amplified detection precision and finds applications in live-cell and tissue imaging, tracking of biomolecules, and drug discovery assays. Reports of their use for in vivo labeling are limited and mostly utilize Tzs with very low speed kinetics ($<10 \text{ M}^{-1} \text{ s}^{-1}$).^{20,21} This leads to very long reaction times or requires intratumoral injections to achieve sufficient ligation at the target site, limiting their clinical applications. Nevertheless, activatable fluorescent probes are highly desired due to their increased TBR, caused by lowering background fluorescence compared to the directly labeled always-on antibodies.^{22–24} A downside of some of the current systems is their reliance on endolysosomal processing and therefore rely on internalization

Received: July 16, 2024

Revised: September 12, 2024

Accepted: September 17, 2024

Published: September 30, 2024



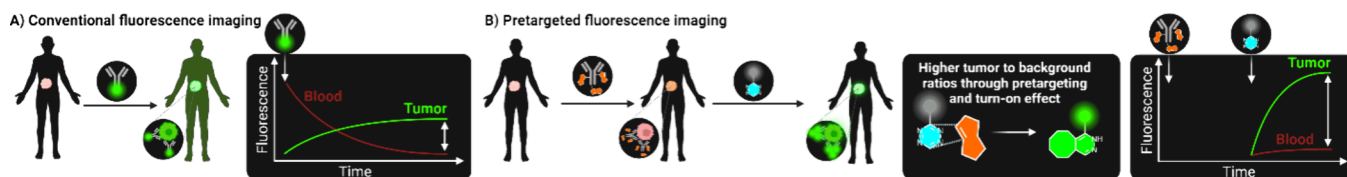


Figure 1. (A) State-of-the-art mAb fluorescence imaging and (B) pretargeting fluorescence imaging based on turn-on BODIPY-tetrazines used in this work.

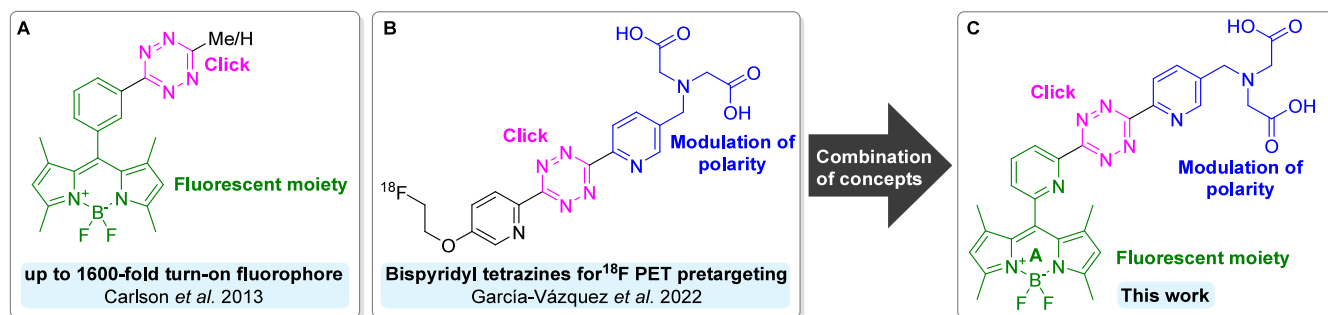
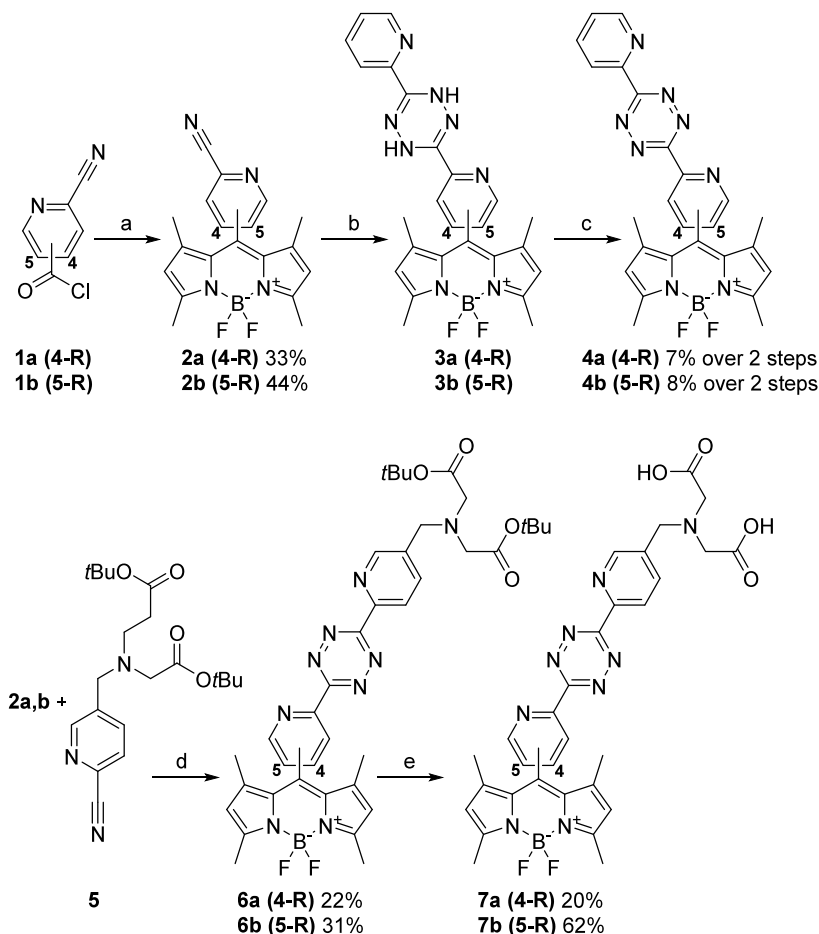


Figure 2. Design of turn-on BODIPY-Tz for pretargeted in vivo fluorescence imaging. (A) Turn-on BODIPY-Tz developed by Carlson et al., (B) ^{18}F -Tz developed by our group with suitable kinetics and polarity for pretargeting, and (C) our design for turn-on BODIPY-Tz with suitable reaction kinetics and polarity for pretargeting.

Scheme 1. Synthesis of BODIPY-Tetrazines^a



^aReaction conditions: (a) 2,4-dimethylpyrrole, DCM, rt, 18 h, then NEt_3 , $\text{BF}_3 \cdot \text{OEt}_2$; (b) 2-cyanopyridine, S_8 , $\text{N}_2\text{H}_4 \cdot \text{H}_2\text{O}$, EtOH, 90 °C, 3–4 h; (c) *p*-chloranil, DCM, rt, 30 min (3a) or $\text{NaNO}_2/\text{AcOH}$, DCM/ H_2O , rt, 30 min (3b); (d) S_8 , $\text{N}_2\text{H}_4 \cdot \text{H}_2\text{O}$, EtOH, 90 °C, 4 h, then *p*-chloranil, DCM, rt, 30 min; (e) 4 M HCl in dioxane, rt, 4 h.

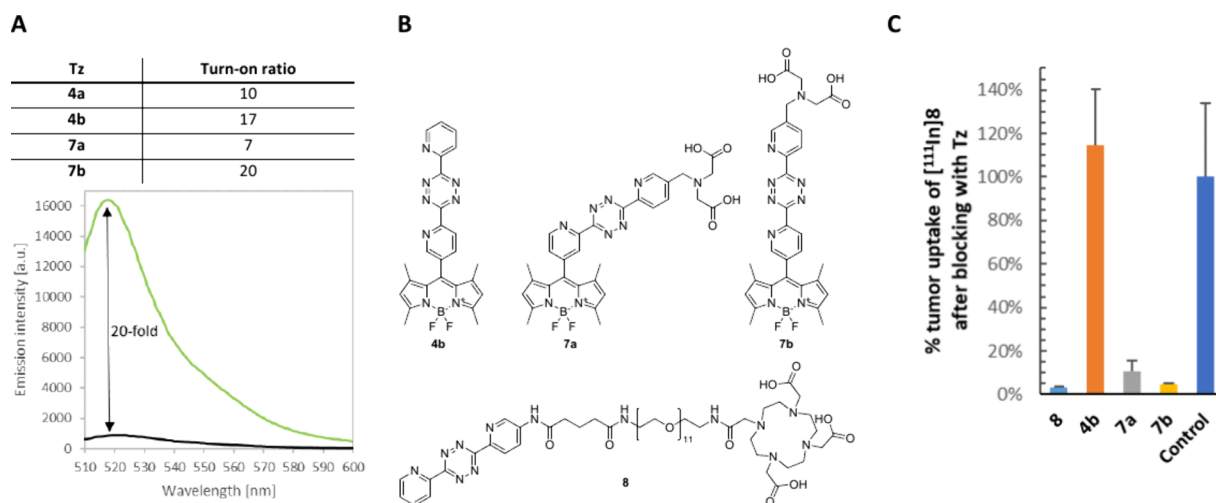


Figure 3. (A) Turn-on ratios of BODIPY-Tzs and exemplary emission spectra of BODIPY-Tz **7b** ($1 \mu\text{M}$) before (black) and after (green) addition of a TCO ($10 \mu\text{M}$) in PBS; excitation at 490 nm . (B) Structures of compounds evaluated in vivo. (C) In vivo blocking effect of **8**, **4b**, **7a**, and **7b**. A lower value indicates a better in vivo performance.

of the targeted cell surface receptors.^{25–27} While probes can also be activated by extracellular enzymes, these enzymes are not overexpressed in cancerous tissues, and the activated fluorophores can diffuse away from the target site.²⁸

In this study, we aimed to develop a pretargeted imaging agent based on a turn-on BODIPY-Tzs with a sufficient rate constant and polarity for in vivo click approaches. Our proof-of-principle study aimed to demonstrate that pretargeted FIGS is indeed possible and can be used as an activatable fluorescent probe to increase the TBR (Figure 1).

RESULTS AND DISCUSSION

Design Strategy. BODIPY-Tzs, reported by the group of Weissleder, were selected as the starting point for the design of our turn-on fluorophores.^{29,30} Especially, the Tzs without a linker (Figure 2A) possess very high turn-on ratios of up to 1600-fold and are promoted by a through-bond energy transfer quenching mechanism rather than the more common, but less effective, Förster resonance energy transfer. Previous results in our group have shown that high reactivities of TCOs ($>50,000 \text{ M}^{-1} \text{ s}^{-1}$) and high hydrophilicity ($\text{cLogD}_{7.4} < -3$) enhance the possibility of a Tz to be used for pretargeted purposes.³¹ While H-Tzs possess such suitable reaction kinetics, the apolar nature of the BODIPY dye scaffold would hamper successful pretargeting. We therefore decided to use bispyridyl Tzs (Figure 2B), which have previously been successfully used in pretargeted radioimmunodiagnosis, as they possess the suitable reaction kinetics and the possibility to introduce polar groups to lower the $\text{cLogD}_{7.4} < -3$.^{32,33} Figure 2C shows the resulting polar BODIPY-Tz. These Tzs should have both suitable kinetics and high enough hydrophilicity to be used for in vivo pretargeting. Another benefit of this design is the late-stage incorporation of both the polar side chain and the BODIPY moiety, minimizing the synthetic steps required on the rather labile Tz moiety.

Tetrazine Synthesis. The synthesis of the corresponding BODIPY-nitrile was achieved through de novo synthesis of the BODIPY moiety using 2-cyanopyridine-4-carbonyl chloride **1a** and 2-cyanopyridine-5-carbonyl chloride **1b** for the respective analogues (Scheme 1). The acid chlorides were reacted with 2 equiv of 2,4-dimethyl-pyrrole in dichloromethane (DCM),

before adding boron trifluoride diethyl etherate and triethyl amine to form the BODIPYs **2a** and **2b**. The Tz synthesis through a pinner-like mechanism was first optimized using 2-cyanopyridine. First, we investigated the use of the catalysts zinc trifluoromethanesulfonate and sulfur to form the Tz core. While sulfur is typically reported for the synthesis of monosubstituted tetrazines, it outperformed $\text{Zn}(\text{OTf})_2$ for the synthesis of BODIPY-Tzs. Attempted direct oxidation of the resulting dihydrotetrazines **3a** and **3b** with aqueous sodium nitrite and acetic acid led to the formation of complex mixtures. Desired Tzs **4a** and **4b** were found to be difficult to isolate, requiring multiple purifications, leading to reduced yields and insufficient purities in the case of **4a**.

We therefore decided to purify the intermediary dihydrotetrazine **3a**. Given the large change in polarity upon the oxidation of **3a** to Tz **4a**, purification was straightforward. Attempted oxidation with commonly employed (diacetoxyiodo)benzene led to decomposition of the BODIPY core. We, therefore, used the milder oxidant *p*-chloranil, leading to full oxidation within a few minutes without noticeable formation of side products. The desired BODIPY-Tzs **4a,b** could be isolated in yields of 7 and 8% over two steps, respectively.

The polar derivatives **7a,b** were synthesized from **2a,b** in a similar fashion, employing the 2-cyanopyridine intermediate **5**.³² **6a,b** could be obtained in 22 and 31% yields and were deprotected in a dioxane solution of hydrochloric acid and purified by preparative HPLC, giving desired polar BODIPY-Tzs **7a,b** in yields of 20 and 62%, respectively.

Physicochemical Characterization. Photophysical properties of the compounds were found to be comparable to the data reported for the methyl- and H-Tz analogues (see the Supporting Information), albeit with a reduced turn-on effect upon the click reaction with axial 5-hydroxy-TCO (Figure 3A). Interestingly, 5-substituted derivatives **4a** and **7a** both showed a higher turn-on effect than their corresponding 4-substituted analogues **4b** and **7b**. This is in contrast to the data reported for the BODIPY-Tzs by Carlson et al., showing the opposite trend. The less efficient quenching of the bispyridyl Tz moiety might be explained by the slight twist of the tetrazine core and pyridyl substituent in bispyridyl Tzs. This could lead to less

efficient overlap of the Tz absorption and BODIPY emission dipole. Despite the lower turn-on ratios compared to literature precedents, we decided to continue the study with the synthesized compounds since multiple attempts to synthesize monosubstituted tetrazines with polar functionalities at the BODIPY core were unsuccessful.

In Vivo Performance/Ex Vivo Blocking. After verifying desirable photophysical properties, we continued to evaluate the in vivo click performance using our in-house developed blocking assay.³¹ This assay employs anti-TAG72 mAb CC49 modified with TCO-tags (CC49-TCO) and ¹¹¹In-labeled compound **8** (Figure 2). In short, LS174T xenograft-bearing mice (expressing TAG72) were injected with CC49-TCO 3 days before the evaluated Tz was injected. Subsequently, [¹¹¹In]**8** was injected 1 h later. This setup allows in vivo comparison of the performance/blocking ability of the evaluated Tz toward [¹¹¹In]**8**. Increased in vivo performance/blocking effect is reflected by lower tumor uptake compared to tumor accumulation of [¹¹¹In]**8** without the Tz under evaluation. This is caused by the evaluated Tz clicking with CC49-TCO at the tumor site and thus blocking the uptake of Tz [¹¹¹In]**8**. In this assay, our polar BODIPY-Tzs **7a** and **7b** showed very low tumor uptake of 10 and 4% and therefore showed excellent blocking effects of 90 and 96%, respectively (Figure 3C). As expected, apolar Tz **4b** showed no blocking effect toward tumor uptake of [¹¹¹In]**8**, confirming that **4b** is not capable of reaching the tumor site in vivo. Compound **4a** could not be evaluated due to observed precipitation during the formulation process. These results are in agreement with our previous findings. Higher hydrophilicity correlates with an increased blocking effect.³¹ Consequently, both Tzs **7a** and **7b** can reach the tumor and ligate specifically to the TCO-bearing mAb.

Ex Vivo Fluorescence Imaging. Given the higher blocking effect and increased turn-on effect of **7b**, we decided to continue to investigate further the biodistribution of this analogue in pretargeted ex vivo fluorescence imaging. Balb/c nude mice bearing LS174T tumor xenografts ($n = 3$ per group) were intravenously injected with either CC49 (control) or CC49-TCO (50 μ g, 0.33 nmol, ~ 3.5 TCOs per mAb). **7b** was injected in a dose of 1:100 (equivalents of TCOs on CC49-TCO to **7b**) in 100 μ L of PBS (pH = 7.4) into the tail vein after 72 h. After 1 h, mice were euthanized, and selected organs were harvested for ex vivo fluorescence measurements (Figure 4). High fluorescence could be observed in the tumor of the pretargeting CC49-TCO group (Figure 4A,B). Tumor-to-organ ratios in the pretargeted CC49-TCO group were generally increased for all organs except the liver. Most importantly, high tumor-to-muscle ratios of around 4 were observed in the CC49-TCO treated group, 2.7-fold higher than those of the control (Figure 4C). The ratiometric threshold for FIGS to determine the presence of cancer is a tumor-to-muscle ratio of 2.7:1.³⁴ Therefore, the obtained results confirm that pretargeted FIGS is feasible. Still, background fluorescence was observed in the absence of TCOs, presumably caused by a combination of metabolized BODIPY-Tz **7b** and tissue autofluorescence at the used excitation wavelength. Especially, high liver uptake was found, a phenomenon previously observed for pretargeting with radiolabeled Tzs.³² However, low muscle and heart (as a surrogate for blood) uptake will allow distinguishing tumor from healthy tissue and will most likely make the developed probe **7b** suitable for FIGS. While the observed TBRs are comparable to those of directly labeled

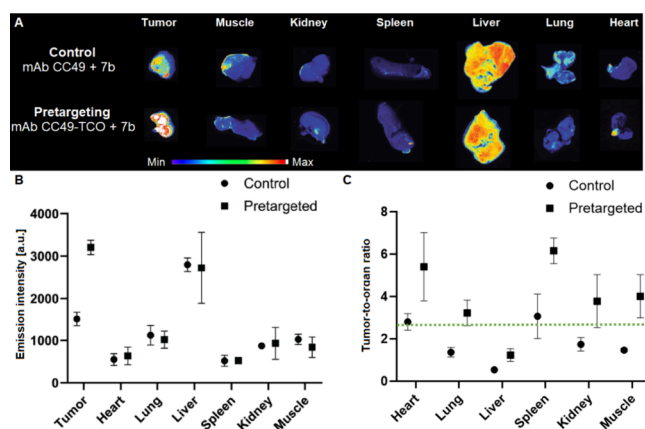


Figure 4. Ex vivo fluorescence evaluation in Balb/c nude mice bearing LS174T tumor xenografts injected with fluorescence at 1:100 dose of TCOs on CC49-TCO to **7b** ($n = 3$). (A) Organs excised from mice injected with nonmodified CC49 and CC49-TCO. (B) Emission intensity per area; error bars indicate SD. (C) Average tumor-to-organ emission intensity ratios; error bars indicate SD. Green dotted line indicates the tumor-to-muscle threshold of 2.7 at which tumor detection through FIGS is feasible.

antibody–dye conjugates, the contribution of the turn-on effect of the dye and pretargeting was not as pronounced as expected (Figure 1). Further optimization of the in vivo stability of the employed Tzs might increase tumor-to-organ ratios even further.

EXPERIMENTAL SECTION

Materials and Methods. In the case where inert conditions were required, the reactions were performed in flame-dried glassware under an inert argon atmosphere. Anhydrous DCM, THF, and DMF were obtained through the use of a PureProcess Technology SG WATER solvent purification system. Chromatographic purification was performed using a Combiflash and prepacked silica gel columns. NMR spectra were acquired using either a 400 MHz Bruker Avance II, equipped with a 5 mm broad band probe, or a 600 MHz Bruker Avance III HD, equipped with a cryogenically cooled 5 mm dual probe optimized for ¹³C and ¹H. Deuterated solvents were used, and the probe was observed at 300 K. LCMS mass spectra were collected using an Agilent 1200 HPLC system, equipped with a Zorbax Eclipse XBD-C18, 4.6 mm \times 50 mm column, an Agilent 6130 mass spectrometer with electron spray ionization (ESI), an autosampler, and a diode array detector. A flow rate of 1 mL/min was used. A linear gradient (0 to 100%) with solvent A (H₂O/MeCN/formic acid, 95:5:0.1 v/v/v) to B (MeCN/formic acid, 100:0:1 v/v/v) was used.

Synthesis of BODIPY-Tetrazines. Preparation of 2a. 2-Cyanoisonicotinoyl chloride (442.2 mg, 2.67 mmol) was dissolved in 40 mL of absolute DCM under an argon atmosphere, and 2,4-dimethylpyrrole (0.5 mL, 462.0 mg, 4.86 mmol) was added. The reaction mixture was stirred at room temperature overnight during which it turned dark red, followed by the addition of triethylamine (2.5 mL) and dropwise addition of BF₃·OEt₂ (2.5 mL) at 0 °C. The reaction was stirred overnight, and 50 mL of water was added to quench the reaction. The phases were separated, and the aqueous phase was extracted twice with 20 mL of DCM. The combined organic phases were washed with saturated aqueous

Na_2CO_3 solution (3 × 20 mL), water (2 × 20 mL), and brine (20 mL), and the organic phase was dried over MgSO_4 . The removal of the solvent furnished a red–brown oil, which was purified by column chromatography (silica gel, toluene), furnishing a red solid (277.2 mg, 0.79 mmol, 33%). ^1H NMR (600 MHz, CDCl_3) δ 8.89 (dt, J = 4.9, 1.0 Hz, 1H), 7.74–7.70 (m, 1H), 7.58–7.53 (m, 1H), 6.04 (s, 2H), 2.56 (s, 6H), 1.39 (s, 6H). ^{13}C NMR (151 MHz, CDCl_3) δ : 157.7, 152.1, 145.5, 142.2, 135.1, 134.8, 130.2, 128.4, 127.0, 122.5, 116.6, 15.1, 14.8.

Preparation of 2b. 6-Cyanonicotinic acid (1.2 g, 8.10 mmol, 1.0 equiv) was suspended in 10 mL of anhydrous toluene, and thionyl chloride (2.29 g, 1.5 mL, 19.04 mmol, 2.35 equiv) was added. The reaction mixture was heated under reflux for 18 h, and the solvents were removed under reduced pressure. The crude product was redissolved in 150 mL of DCM, and 2,4-dimethylpyrrole (1.54 g, 1.67 mL, 16.20 mmol, 2.0 equiv) was added. The resulting solution was stirred overnight during which it turned deep red. The reaction mixture was cooled to 0 °C in an ice bath, and triethylamine (6.05 g, 8.34 mL, 59.8 mmol, 7.38 equiv) was added, followed by dropwise addition of $\text{BF}_3 \cdot \text{OEt}_2$ (9.43 g, 8.34 mL, 66.41 mmol, 8.20 equiv). After being stirred overnight, the deep orange reaction mixture was quenched by the addition of 100 mL of 2N Na_2CO_3 solution. After stirring for 10 min, the phases were separated, and the organic phase was washed with 2N Na_2CO_3 solution (2 × 100 mL), water (3 × 100 mL), and brine (100 mL). The organic phase was dried over MgSO_4 , and the solvent was removed under reduced pressure. Flash column chromatography (silica gel, toluene) furnished a red solid (1.25 g, 3.56 mmol, 44%). ^1H NMR (400 MHz, CDCl_3) δ 8.79–8.63 (m, 1H), 7.94–7.77 (m, 2H), 6.04 (s, 2H), 2.56 (s, 6H), 1.36 (s, 6H). ^{13}C NMR (101 MHz, CDCl_3) δ : 157.5, 150.4, 142.4, 137.5, 135.1, 134.8, 134.5, 131.1, 128.5, 122.4, 116.8, 15.4, 14.8.

Preparation of 4a. Compound 2a (250.0 mg, 0.71 mmol, 1.0 equiv), 2-cyanopyridine (1.04 g, 9.97 mmol, 14.0 equiv), and sulfur (91.3 mg, 0.36 mmol, 0.5 equiv) were suspended in 20.0 mL of EtOH under an argon atmosphere, and hydrazine hydrate (1.04 mL, 1.07 g, 21.36 mmol, 30.0 equiv) was added dropwise. The reaction was heated to reflux, leading to rapid gas formation, which was allowed to escape by piercing the septum on top of the reflux condenser with two needles. After 4 h of reflux, the reaction was cooled to room temperature, and 100 mL of DCM and 100 mL of water were added. The phases were separated, and the organic phase was washed twice with 100 mL of water and once with 100 mL of brine. The organic phase was dried over MgSO_4 , and the solvent was removed under reduced pressure, furnishing a deep red solid. The thus obtained crude product was purified by flash column chromatography (silica gel, 0 to 5% EtOAc in DCM v/v), yielding an orange solid. The solid was redissolved in 5 mL of DCM, and *p*-chloranil (28.4 mg, 0.12 mmol) was added. The reaction mixture was stirred for 10 min, and Celite was added. The solvent was removed under reduced pressure, and the crude product was purified by automated flash column chromatography (silica gel, 0 to 50% EtOAc in DCM, v/v). The product was obtained as a deep orange solid (25.0 mg, 5.2 μmol , 7%). ^1H NMR (600 MHz, CDCl_3) δ 9.15 (d, J = 4.8 Hz, 1H), 9.02 (dd, J = 4.8, 1.6 Hz, 1H), 8.81–8.73 (m, 2H), 8.03 (td, J = 7.8, 1.7 Hz, 1H), 7.65–7.57 (m, 2H), 6.05 (s, 2H), 2.59 (s, 6H), 1.49 (s, 6H). ^{11}B NMR (128 MHz, CDCl_3) δ 0.70 (t, J = 32.5 Hz). ^{13}C NMR (151 MHz, CDCl_3) δ : 164.1,

163.7, 157.2, 152.0, 151.4, 151.3, 150.0, 145.6, 142.6, 137.7, 136.6, 130.5, 127.0, 126.4, 124.9, 124.3, 122.3, 15.2, 14.9. ^{19}F NMR (376 MHz, CDCl_3) δ –145.57–146.75 (m). ESI-MS (m/z) calcd. for $[\text{M} + \text{H}]^+$ = 483.2; found 483.2.

Preparation of 4b. Compound 2b (200.0 mg, 0.67 mmol, 1.0 equiv), 2-cyanopyridine (118.6 mg, 1.14 mmol, 2.0 equiv), and sulfur (36.5 mg, 0.14 mmol, 0.25 equiv) were suspended in 1.2 mL of EtOH under an argon atmosphere, and hydrazine hydrate (555.2 μL , 570.2 mg, 11.4 mmol, 20.0 equiv) was added dropwise. The reaction was heated to reflux, leading to rapid gas formation, which was allowed to escape by piercing the septum on top of the reflux condenser with two needles. After 3 h, the solution was cooled to room temperature and used in the oxidation step as is. The reaction mixture was poured into 300 mg of NaNO_2 in 10 mL of water, and the reaction vessel was washed with DCM and poured into the aqueous mixture. AcOH (approximately 4 mL) was added carefully under heavy stirring. After 10 min, 10 mL of DCM was added, and the phases were separated. The aqueous phase was extracted with 10 mL of DCM, and the combined organic phases were washed thrice with 15 mL of water. The organic phase was dried over MgSO_4 , and the solvent was removed under reduced pressure, furnishing a deep red solid. The crude product was purified by flash column chromatography on silica gel using an eluent of DCM to DCM/EtOAc 4:1 v/v. The desired product was obtained as a deep red solid (11.1 mg, 23.0 μmol , 8%). ^1H NMR (400 MHz, CDCl_3) δ 9.01 (d, J = 4.0 Hz, 1H), 8.95 (d, J = 8.2 Hz, 2H), 8.08–7.97 (m, 2H), 7.61 (ddd, J = 7.7, 4.7, 1.1 Hz, 1H), 6.05 (s, 2H), 2.59 (s, 6H), 1.48 (s, 6H). ^{11}B NMR (128 MHz, CDCl_3) δ 0.74 (t, J = 32.3 Hz). ^{13}C NMR (101 MHz, CDCl_3) δ : 164.1, 163.6, 157.1, 151.3, 150.7, 150.2, 150.0, 142.7, 138.0, 137.7, 136.1, 134.7, 131.4, 126.9, 124.9, 124.5, 122.2, 15.5, 14.8. ^{19}F NMR (376 MHz, CDCl_3) δ –146.07 (q, J = 32.3 Hz), –146.16 (q, J = 32.3 Hz). ESI-MS (m/z) calcd. for $[\text{M} + \text{H}]^+$ = 483.2; found 483.2.

Preparation of 6a. Compound 2a (100.0 mg, 0.28 mmol, 1.0 equiv), di-*tert*-butyl 2,2'-(((6-cyanopyridin-3-yl)methyl)-azanediyl)diacetate (1.03 g, 2.85 mmol, 10.0 equiv), and sulfur (36.5 mg, 0.14 mmol, 0.5 equiv) were suspended in 10.0 mL of EtOH under an argon atmosphere, and hydrazine hydrate (416.4 μL , 427.6 mg, 8.54 mmol, 30.0 equiv) was added dropwise. The reaction was heated to reflux, leading to rapid gas formation, which was allowed to escape by piercing the septum on top of the reflux condenser with two needles. After 4 h of reflux, the reaction was cooled to room temperature, and 40 mL of DCM and 40 mL of water were added. After adding a small amount of brine to aid in phase separation, the phases were separated, and the organic phase was washed twice with 40 mL of water and once with 40 mL of brine. The organic phase was dried over MgSO_4 , and the solvent was removed under reduced pressure, furnishing a deep red solid. The thus obtained crude product was purified by flash column chromatography (silica gel, 0 to 4% EtOAc in DCM v/v), yielding an orange oil. The obtained oil (228.4 mg) was redissolved in 5 mL of DCM, and *p*-chloranil (83.2 mg) was added. The solution was stirred for 10 min at rt. The solvent was removed under reduced pressure, and the crude product was purified by automated flash column chromatography (silica gel, EtOAc in DCM, 0 to 30% v/v). The desired product was obtained as a red solid (46.3 mg, 62.6 μmol , 22%). ^1H NMR (400 MHz, CDCl_3) δ 9.13 (d, J = 4.9 Hz, 1H), 8.90 (d, J = 2.0 Hz, 1H), 8.76 (s, 1H), 8.72 (d, J = 8.1

Hz, 1H), 8.21 (dd, $J = 8.1, 2.1$ Hz, 1H), 7.59 (dd, $J = 4.8, 1.6$ Hz, 1H), 6.03 (s, 2H), 4.09 (s, 2H), 3.47 (s, 4H), 2.57 (s, 6H), 1.49–1.43 (m, 24H). ^{11}B NMR (128 MHz, CDCl_3) δ 0.71 (t, $J = 32.6$ Hz). ^{13}C NMR (151 MHz, CDCl_3) δ : 170.4, 164.2, 163.7, 157.2, 151.9, 151.6, 151.4, 149.1, 145.6, 142.6, 138.6, 138.5, 136.7, 130.5, 126.3, 124.7, 124.2, 122.3, 81.6, 55.5, 54.8, 28.3, 15.2, 14.9. ^{19}F NMR (376 MHz, CDCl_3) δ -146.08 (q, $J = 32.6$ Hz), -146.17 (q, $J = 32.6$ Hz). ESI-MS (m/z) calcd. for $[\text{M} + \text{H}]^+ = 740.4$; found 740.3.

Preparation of 6b. Compound **2b** (100.0 mg, 0.28 mmol, 1.0 equiv), di-*tert*-butyl 2,2'-((6-cyanopyridin-3-yl)methyl)-azanediyl)diacetate (1.03 g, 2.85 mmol, 10.0 equiv), and sulfur (36.5 mg, 0.14 mmol, 0.5 equiv) were suspended in 10.0 mL of EtOH under an argon atmosphere, and hydrazine hydrate (416.4 μL , 427.6 mg, 8.54 mmol, 30.0 equiv) was added dropwise. The reaction was heated to reflux, leading to rapid gas formation, which was allowed to escape by piercing the septum on top of the reflux condenser with two needles. After 4 h of reflux, the reaction was cooled to room temperature, and 40 mL of DCM and 40 mL of water were added. After adding a small amount of brine to aid in phase separation, the phases were separated, and the organic phase was washed twice with 40 mL of water and once with 40 mL of brine. The organic phase was dried over MgSO_4 , and the solvent was removed under reduced pressure, furnishing a deep red solid. The thus obtained crude product was purified by flash column chromatography (silica gel, 0 to 4% EtOAc in DCM v/v), yielding an orange oil. The obtained oil (102.0 mg) was dissolved in 5 mL of DCM, and *p*-chloranil (104.8 mg) was added. The solution was stirred for 10 min at rt. The solvent was removed under reduced pressure, and the crude product was purified by automated flash column chromatography (silica gel, EtOAc in DCM, 0 to 30% v/v). Red solid (65.0 mg, 87.8 μmol , 31%). ^1H NMR (600 MHz, CDCl_3) δ 8.96–8.90 (m, 3H), 8.74 (d, $J = 8.0$ Hz, 1H), 8.24 (dd, $J = 8.1, 2.1$ Hz, 1H), 8.00 (dd, $J = 8.0, 2.2$ Hz, 1H), 6.04 (s, 2H), 4.12 (s, 2H), 3.49 (s, 4H), 2.58 (s, 6H), 1.49–1.46 (m, 24H). ^{11}B NMR (128 MHz, CDCl_3) δ 0.74 (t, $J = 32.7$ Hz). ^{13}C NMR (151 MHz, CDCl_3) δ : 170.1, 164.1, 163.6, 157.1, 151.6, 150.7, 150.1, 149.2, 142.7, 138.6, 138.2, 137.9, 136.2, 134.6, 131.4, 124.8, 124.4, 122.2, 81.7, 55.3, 54.8, 28.3, 15.4, 14.8. ^{19}F NMR (376 MHz, CDCl_3) δ -145.46–-146.69 (m). ESI-MS (m/z) calcd. for $[\text{M} + \text{H}]^+ = 740.4$; found 740.3.

Preparation of 7a. Compound **6a** (11.4 mg, 15.4 μmol) was dissolved in 2 mL of 4 M HCl in dioxane at 0 $^\circ\text{C}$. The reaction mixture was warmed to room temperature and stirred for 4 h. The solvent was removed under reduced pressure, furnishing a red solid. The crude product was redissolved in 5 mL of MeCN/ H_2O (1:1 v/v, 0.1% TFA) and purified by preparative HPLC, furnishing a red solid (1.9 mg, 3.0 μmol , 20%). ^1H NMR (600 MHz, CD_3OD) δ 9.09 (dd, $J = 4.9, 0.9$ Hz, 1H), 8.95 (d, $J = 2.5$ Hz, 1H), 8.82–8.76 (m, 2H), 8.28 (dd, $J = 8.1, 2.2$ Hz, 1H), 7.85 (dd, $J = 4.9, 1.6$ Hz, 1H), 6.15 (s, 2H), 4.24 (s, 2H), 3.71 (s, 4H), 2.52 (s, 6H), 1.53 (s, 6H). ^{11}B NMR (128 MHz, CD_3OD) δ 4.65 (t, $J = 31.9$ Hz). ^{13}C NMR (151 MHz, CD_3OD) δ : 173.6, 164.9, 164.8, 158.1, 152.7, 152.6, 152.4, 150.4, 146.9, 144.1, 140.6, 138.8, 138.5, 131.5, 128.2, 125.6, 125.6, 123.1, 56.4, 55.4, 15.2, 14.6. ^{19}F NMR (376 MHz, CD_3OD) δ -143.09 (q, $J = 31.5$ Hz). ESI-MS (m/z) calcd. for $[\text{M} + \text{H}]^+ = 628.2$; found 628.2.

Preparation of 7b. Compound **6b** (31.6 mg, 42.7 μmol , 1.0 equiv) was dissolved in 7 mL of 4 M HCl in dioxane and stirred for 3.5 h. The solvent was removed under reduced

pressure, furnishing a red solid. The crude product was redissolved in 5 mL of MeCN/ H_2O (1:1 v/v, 0.1% TFA) and purified by preparative HPLC to furnish a red solid (16.7 mg, 26.6 μmol , 62%). ^1H NMR (600 MHz, DMSO) δ 12.43 (brs, 2H), 9.02 (dd, $J = 2.2, 0.9$ Hz, 1H), 8.91 (d, $J = 2.0$ Hz, 1H), 8.81 (dd, $J = 8.0, 0.9$ Hz, 1H), 8.63–8.59 (m, 1H), 8.30 (dd, $J = 8.0, 2.2$ Hz, 1H), 8.15 (dd, $J = 8.1, 2.2$ Hz, 1H), 6.27 (s, 2H), 4.06 (s, 2H), 3.52 (s, 4H), 1.45 (s, 6H). Two CH_3 groups were under the residual solvent peak. ^{11}B NMR (128 MHz, DMSO) δ 0.63 (t, $J = 32.8$ Hz). ^{13}C NMR (151 MHz, DMSO) δ : 172.2, 163.2, 162.9, 155.8, 150.9, 150.7, 149.3, 148.9, 142.6, 138.2, 138.1, 137.7, 137.2, 132.9, 130.7, 124.2, 124.1, 122.0, 54.5, 54.0, 14.8, 14.3. ^{19}F NMR (376 MHz, DMSO) δ -143.53 (q, $J = 31.6$ Hz). ESI-MS (m/z) calcd. for $[\text{M} + \text{H}]^+ = 628.2$; found 628.2.

Turn-On Measurements. Turn-on ratios were determined on a Tecan Safire² plate reader. 1 mM stock solutions in DMSO of the BODIPY-Tzs **4a**, **4b**, **7a**, and **7b** were diluted in PBS (pH = 7.4) to yield 1 μM final concentrations of the fluorophore. Fluorescence spectra were collected by using an excitation wavelength of 490 nm. A 10 mM stock solution of axial (*E*)-cyclooct-4-en-1-ol in DMSO was added (10-fold excess, final concentration 10 μM), and the fluorescence spectra were measured again under the same settings (see Figures S1–S4). Turn-on ratios were determined by comparison of the average emission intensity maximum of the clicked products (517 nm, $n = 3$) to the corresponding emission intensity of **4a**, **4b**, **7a**, and **7b** at the same wavelength.

In Vivo Evaluation. All animal experiments were performed, according to the directive 2010/63/EU of the European Parliament and the European Council on the protection of animals used for scientific purposes, and were approved by the Danish Animal Experiments Inspectorate under an approved animal license (2021-15-0201-01041), approved December 2021.

In vivo evaluation was carried out with balb/c-Foxn1 nude mice carrying subcutaneous LS174T flank xenografts. Briefly, LS174T cells were cultivated according to ATCC guidelines, with the addition of penicillin and streptomycin. Cells were harvested by trypsinase and washed in PBS by spinning at 400 RCF for 5 min. After reconstitution in PBS, mice were injected with 5×10^6 cells subcutaneously on the left flank. After approximately 7–10 days, mice were injected with CC49 or CC49-TCO in PBS.

For blocking experiments, mice injected with CC49-TCO 72 h prior were injected with saline (positive control), unlabeled DOTA-Tz **8** (negative control), **4b**, **7a** or **7b** ($n = 3$ per compound). One hour after injection of each nonradiolabeled tetrazine, mice were injected with [^{111}In]In-**8**. Twenty-two hours later, mice were euthanized, and tumor, blood, liver, spleen, kidney, heart, lung, and muscle organs/tissues were resected and weighed, and the ^{111}In content was determined using a Wizard 2 automatic gamma counter (PerkinElmer, USA). %ID/g was calculated by dividing the decay-corrected organ ^{111}In activity uptake by the injected dose and organ mass. The tumor blocking effect of nonradiolabeled tetrazines was assessed as the change in tumor uptake of [^{111}In]In-x relative to the positive control.

From the blocking experiment described above, **7b** was selected for the ex vivo fluorescence assessment. Mice carrying LS174T xenografts of $\sim 90 \text{ mm}^3$ were injected with CC49 or CC49-TCO ($n = 3$ each group). 72 h later, mice were injected

with 7b, and 1 h after injection, animals were euthanized, and tumor, liver, spleen, kidney, heart, lung, and muscle were resected and subsequently fluorescence-imaged using a typhoon biomolecular imager (Cytiva, USA), with a 488 nm excitation, a 525/20 emission filter, and a 322 V PMT voltage. Regions of interest were drawn along the contour of all organs using ImageQuantTL 8.2 (GE Healthcare, USA), and the average absolute fluorescence intensity was reported.

CONCLUSIONS

The synthesis route toward two polar, aqueous soluble BODIPY-Tzs with rapid bioorthogonal kinetics was developed. In vivo pretargeted fluorescence imaging of LS174T tumor xenografts using preaccumulated CC49-TCO antibodies succeeded. Tumor-to-muscle ratios of 4:1 are comparable to those of directly labeled antibodies, confirming successful pretargeting with the synthesized dyes. Increasing the metabolic stability of the fluorophore Tzs, as well as the use of clearing or masking agents, might lead to even higher tumor-to-organ ratios. This proof-of-concept study indicates that pretargeting with polar Tz-based dyes could, in the future, be applied toward pretargeted photodynamic and -thermal therapies. Such an approach could lead to severely reduced side effects due to decreased exposure to the dyes compared to directly labeled antibody–dye conjugates.

ASSOCIATED CONTENT

Supporting Information

The Supporting Information is available free of charge at <https://pubs.acs.org/doi/10.1021/acsomega.4c06570>.

Emission spectra of turn-on measurements, copies of the ^1H and ^{13}C NMR spectra of synthesized compounds, and HPLC chromatograms of compounds evaluated in vivo (PDF)

AUTHOR INFORMATION

Corresponding Authors

Andreas Kjær – Department of Clinical Physiology, Nuclear Medicine & PET, 2100 Copenhagen, Denmark; Cluster for Molecular Imaging, Department of Biomedical Sciences, University of Copenhagen, 2100 Copenhagen, Denmark; orcid.org/0000-0002-2706-5547; Email: akjaer@sund.ku.dk

Matthias M. Herth – Department of Drug Design and Pharmacology, Faculty of Health and Medical Sciences, University of Copenhagen, 2100 Copenhagen, Denmark; Department of Clinical Physiology, Nuclear Medicine & PET, 2100 Copenhagen, Denmark; orcid.org/0000-0002-7788-513X; Email: matthias.herth@sund.ku.dk

Authors

Markus Staudt – Department of Drug Design and Pharmacology, Faculty of Health and Medical Sciences, University of Copenhagen, 2100 Copenhagen, Denmark; orcid.org/0000-0002-7712-1818

Lars Hvass – Department of Clinical Physiology, Nuclear Medicine & PET, 2100 Copenhagen, Denmark; Cluster for Molecular Imaging, Department of Biomedical Sciences, University of Copenhagen, 2100 Copenhagen, Denmark

Marius Müller – Department of Drug Design and Pharmacology, Faculty of Health and Medical Sciences,

University of Copenhagen, 2100 Copenhagen, Denmark;

orcid.org/0000-0003-1882-5919

Rocío García-Vázquez – Department of Drug Design and Pharmacology, Faculty of Health and Medical Sciences, University of Copenhagen, 2100 Copenhagen, Denmark

Jesper Tranekjær Jørgensen – Department of Clinical Physiology, Nuclear Medicine & PET, 2100 Copenhagen, Denmark; Cluster for Molecular Imaging, Department of Biomedical Sciences, University of Copenhagen, 2100 Copenhagen, Denmark

Vladimir Shalgunov – Department of Drug Design and Pharmacology, Faculty of Health and Medical Sciences, University of Copenhagen, 2100 Copenhagen, Denmark; Department of Clinical Physiology, Nuclear Medicine & PET, 2100 Copenhagen, Denmark; orcid.org/0000-0001-8956-1207

Umberto Maria Battisti – Department of Drug Design and Pharmacology, Faculty of Health and Medical Sciences, University of Copenhagen, 2100 Copenhagen, Denmark; orcid.org/0000-0002-1012-8644

Complete contact information is available at: <https://pubs.acs.org/10.1021/acsomega.4c06570>

Notes

The authors declare no competing financial interest.

ACKNOWLEDGMENTS

This project has received funding from Danmarks Frie Forskningsfond under Grant No. 2035-00077B. The graphical abstract and Figure 1 were created with [BioRender.com](https://www.biorender.com).

REFERENCES

- (1) Lee, J. Y. K.; Cho, S. S.; Stummer, W.; Tanyi, J. L.; Vahrmeijer, A. L.; Rosenthal, E.; Smith, B.; Henderson, E.; Roberts, D. W.; Lee, A.; Hadjipanayis, C. G.; Bruce, J. N.; Newman, J. G.; Singhal, S. Review of Clinical Trials in Intraoperative Molecular Imaging during Cancer Surgery. *J. Biomed. Opt.* **2019**, *24*, 1.
- (2) Hernot, S.; van Manen, L.; Debie, P.; Mieog, J. S. D.; Vahrmeijer, A. L. Latest Developments in Molecular Tracers for Fluorescence Image-Guided Cancer Surgery. *Lancet Oncol.* **2019**, *20*, e354–e367.
- (3) Nagaya, T.; Nakamura, Y. A.; Choyke, P. L.; Kobayashi, H. Current and New Fluorescent Probes for Fluorescence-Guided Surgery. *Strat. Curative Fluoresc. Surg. Cancer* **2020**, *75*–114.
- (4) Li, X.; Lovell, J. F.; Yoon, J.; Chen, X. Clinical Development and Potential of Photothermal and Photodynamic Therapies for Cancer. *Nat. Rev. Clin. Oncol.* **2020**, *17*, 657–674.
- (5) Gunaydin, G.; Gedik, M. E.; Ayan, S. Photodynamic Therapy for the Treatment and Diagnosis of Cancer—A Review of the Current Clinical Status. *Front. Chem.* **2021**, *9*, No. 686303.
- (6) Rosenthal, E. L.; Warram, J. M.; De Boer, E.; Chung, T. K.; Korb, M. L.; Brandwein-Gensler, M.; Strong, T. V.; Schmalbach, C. E.; Morlandt, A. B.; Agarwal, G.; Hartman, Y. E.; Carroll, W. R.; Richman, J. S.; Clemons, L. K.; Nabell, L. M.; Zinn, K. R. Safety and Tumor Specificity of Cetuximab-IRDye800 for Surgical Navigation in Head and Neck Cancer. *Clin. Cancer Res.* **2015**, *21*, 3658–3666.
- (7) Gong, L.; Ding, H.; Long, N. E.; Sullivan, B. J.; Martin, E. W.; Magliery, T. J.; Tweedle, M. F. A 3E8.ScFv.Cys-IR800 Conjugate Targeting TAG-72 in an Orthotopic Colorectal Cancer Model. *Mol. Imaging Biol.* **2018**, *20*, 47–54.
- (8) Ormond, A. B.; Freeman, H. S. Dye Sensitizers for Photodynamic Therapy. *Materials. Multidisciplinary Digital Publishing Institute* **2013**, *6*, 817–840.

- (9) Trehan, M.; Taylor, C. R. Chapter 21 Cutaneous Photo-sensitivity and Photoprotection for Photodynamic Therapy Patients. *Compr. Ser. Photosciences* **2001**, *2*, 321–337.
- (10) Rijpkema, M.; Bos, D. L.; Cornelissen, A. S.; Franssen, G. M.; Goldenberg, D. M.; Oyen, W. J.; Boerman, O. C. Optimization of Dual-Labeled Antibodies for Targeted Intraoperative Imaging of Tumors. *Mol. Imaging* **2015**, *14*, 348–355.
- (11) Szabó, Á.; Szendi-Szalmáry, T.; Ujlaky-Nagy, L.; Rádi, I.; Vereb, G.; Szöllösi, J.; Nagy, P. The Effect of Fluorophore Conjugation on Antibody Affinity and the Photophysical Properties of Dyes. *Biophys. J.* **2018**, *114*, 688–700.
- (12) Cilliers, C.; Nessler, I.; Christodolu, N.; Thurber, G. M. Tracking Antibody Distribution with Near-Infrared Fluorescent Dyes: Impact of Dye Structure and Degree of Labeling on Plasma Clearance. *Mol. Pharmaceutics* **2017**, *14*, 1623–1633.
- (13) Ahn, S. H.; Boros, E. Nuclear and Optical Bimodal Imaging Probes Using Sequential Assembly: A Perspective. *Cancer Biother. Radiopharm.* **2018**, *33*, 308–315.
- (14) García-Vázquez, R.; Battisti, U.; Herth, M. Recent Advances in the Development of Tetrazine Ligation Tools for Pretargeted Nuclear Imaging. *Pharmaceutics* **2022**, *15*, 685.
- (15) Staudt, M.; Herth, M.; Poulie, C. B. M. Pretargeted Theranostics. In *Theranostics - An Old Concept in New Clothing*; IntechOpen, 2021.
- (16) Stéen, E. J. L.; Edem, P. E.; Nørregaard, K.; Jørgensen, J. T.; Shalgunov, V.; Kjaer, A.; Herth, M. M. Pretargeting in Nuclear Imaging and Radionuclide Therapy: Improving Efficacy of Theranostics and Nanomedicines. *Biomaterials* **2018**, *179*, 209–245.
- (17) Staudt, M.; Herth, M. M. Clearing and Masking Agents in Pretargeting Strategies. *Pharmaceutics* **2023**, *16*, 497.
- (18) Oliveira, B. L.; Guo, Z.; Bernardes, G. J. L. Inverse Electron Demand Diels-Alder Reactions in Chemical Biology. *Chem. Soc. Rev.* **2017**, *14*, 4895–4950.
- (19) Loredó, A.; Tang, J.; Wang, L.; Wu, K. L.; Peng, Z.; Xiao, H. Tetrazine as a General Phototrigger to Turn on Fluorophores. *Chem. Sci.* **2020**, *11*, 4410–4415.
- (20) Mao, W.; Tang, J.; Dai, L.; He, X.; Li, J.; Cai, L.; Liao, P.; Jiang, R.; Zhou, J.; Wu, H. A General Strategy to Design Highly Fluorogenic Far-Red and Near-Infrared Tetrazine Bioorthogonal Probes. *Angew. Chem. Int. Ed.* **2021**, *60*, 2393–2397.
- (21) Mao, W.; Chi, W.; He, X.; Wang, C.; Wang, X.; Yang, H.; Liu, X.; Wu, H. Overcoming Spectral Dependence: A General Strategy for Developing Far-Red and Near-Infrared Ultra-Fluorogenic Tetrazine Bioorthogonal Probes. *Angew. Chem., Int. Ed.* **2022**, *61*, No. e202117386.
- (22) Kobayashi, H.; Choyke, P. L. Target-Cancer-Cell-Specific Activatable Fluorescence Imaging Probes: Rational Design and in Vivo Applications. *Acc. Chem. Res.* **2011**, *44*, 83–90.
- (23) Urano, Y. Novel Live Imaging Techniques of Cellular Functions and in Vivo Tumors Based on Precise Design of Small Molecule-Based 'Activatable' Fluorescence Probes. *Curr. Opin. Chem. Biol.* **2012**, *16*, 602–608.
- (24) Kobayashi, H.; Ogawa, M.; Alford, R.; Choyke, P. L.; Urano, Y. New Strategies for Fluorescent Probe Design in Medical Diagnostic Imaging. *Chem. Rev.* **2010**, *110*, 2620–2640.
- (25) Hama, Y.; Urano, Y.; Koyama, Y.; Kamiya, M.; Bernardo, M.; Paik, R. S.; Shin, I. S.; Paik, C. H.; Choyke, P. L.; Kobayashi, H. A Target Cell-Specific Activatable Fluorescence Probe for in Vivo Molecular Imaging of Cancer Based on a Self-Quenched Avidin-Rhodamine Conjugate. *Cancer Res.* **2007**, *67*, 2791–2799.
- (26) Mahmood, U.; Tung, C. H.; Bogdanov, A.; Weissleder, R. Near-Infrared Optical Imaging of Protease Activity for Tumor Detection. *Radiology* **1999**, *213*, 866–870.
- (27) Tung, C. H.; Bredow, S.; Mahmood, U.; Weissleder, R. Preparation of a Cathepsin D Sensitive Near-Infrared Fluorescence Probe for Imaging. *Bioconjugate Chem.* **1999**, *10*, 892–896.
- (28) Nagaya, T.; Nakamura, Y. A.; Choyke, P. L.; Kobayashi, H. Fluorescence-Guided Surgery. *Front. Oncol.* **2017**, *22*, 314.
- (29) Devaraj, N. K.; Hilderbrand, S.; Upadhyay, R.; Mazitschek, R.; Weissleder, R. Bioorthogonal Turn-on Probes for Imaging Small Molecules inside Living Cells. *Angew. Chemie - Int. Ed.* **2010**, *49*, 2869–2872.
- (30) Carlson, J. C. T.; Meimetis, L. G.; Hilderbrand, S. A.; Weissleder, R. BODIPY-Tetrazine Derivatives as Superbright Bioorthogonal Turn-on Probes. *Angew. Chemie - Int. Ed.* **2013**, *52*, 6917–6920.
- (31) Stéen, E. J. L.; Jørgensen, J. T.; Denk, C.; Battisti, U. M.; Nørregaard, K.; Edem, P. E.; Bratteby, K.; Shalgunov, V.; Wilkovitsch, M.; Svatunek, D.; Poulie, C. B. M.; Hvass, L.; Simón, M.; Wanek, T.; Rossin, R.; Robillard, M.; Kristensen, J. L.; Mikula, H.; Kjaer, A.; Herth, M. M. Lipophilicity and Click Reactivity Determine the Performance of Bioorthogonal Tetrazine Tools in Pretargeted in Vivo Chemistry. *ACS Pharmacol. Transl. Sci.* **2021**, *4*, 824–833.
- (32) García-Vázquez, R.; Jørgensen, J. T.; Bratteby, K. E.; Shalgunov, V.; Hvass, L.; Herth, M. M.; Kjaer, A.; Battisti, U. M. Development of 18F-Labeled Bispyridyl Tetrazines for In Vivo Pretargeted PET Imaging. *Pharmaceutics* **2022**, *15*, 245.
- (33) Edem, P. E.; Jørgensen, J. T.; Nørregaard, K.; Rossin, R.; Yazdani, A.; Valliant, J. F.; Robillard, M.; Herth, M. M.; Kjaer, A. Evaluation of a 68Ga-Labeled DOTA-Tetrazine as a PET Alternative to 111In-SPECT Pretargeted Imaging. *Molecules* **2020**, *25*, 463.
- (34) Warram, J. M.; De Boer, E.; Moore, L. S.; Schmalbach, C. E.; Withrow, K. P.; Carroll, W. R.; Richman, J. S.; Morlandt, A. B.; Brandwein-Gensler, M.; Rosenthal, E. L. A Ratiometric Threshold for Determining Presence of Cancer during Fluorescence-Guided Surgery. *J. Surg. Oncol.* **2015**, *112*, 2–8.